Article

Metal-Assembling Dendrimers with a Triarylamine Core and Their Application to a Dye-Sensitized Solar Cell

Norifusa Satoh, Toshio Nakashima, and Kimihisa Yamamoto

J. Am. Chem. Soc., **2005**, 127 (37), 13030-13038• DOI: 10.1021/ja050765c • Publication Date (Web): 26 August 2005

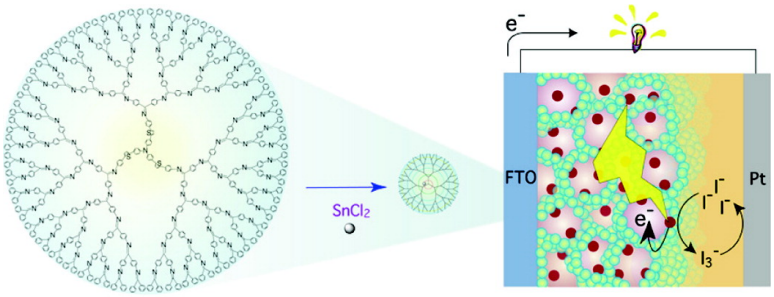

More About This Article

Additional resources and features associated with this article are available within the HTML version:

- Supporting Information
- Links to the 18 articles that cite this article, as of the time of this article download
- Access to high resolution figures
- Links to articles and content related to this article
- Copyright permission to reproduce figures and/or text from this article

View the Full Text HTML

J|A|C|S
ARTICLES
Published on Web 08/26/2005

Metal-Assembling Dendrimers with a Triarylamine Core and Their Application to a Dye-Sensitized Solar Cell

Norifusa Satoh, Toshio Nakashima, and Kimihisa Yamamoto*

Contribution from the Department of Chemistry, Faculty of Science & Technology, Keio University, Yokohama 223-8522, Japan

Received February 4, 2005; E-mail: yamamoto@chem.keio.ac.jp

Abstract: A series of charge-separable and hole-transporting phenylazomethine dendrimers with a triarylamine core are prepared and evaluated for use as a charge separator in dye-sensitized solar cells (DSSCs). Triphenylamine with dendric phenylazomethine (TPA-DPA) is prepared by synthesizing up to five generations of dendrons using a convergent method. The resultant dendrimer has a rigid sphere structure similar to globular protein, with a hydrodynamic radius of 2.43 nm. Electrochemical oxidation of the TPA core reveals that the dendron units in the dendrimer have 0.35 of the attenuation factor (β) in the electron transfer. Complexation of TPA-DPA with $SnCl_2$ proceeds in stepwise fashion from the core to the terminal imine following the basicity gradient among imine groups in each dendron shell. DSSCs prepared by casting these dendrimers onto dye-sensitized TiO_2 film exhibited a higher open-circuit voltage than the bare film through the suppression of back electron transfer. The generational growth of dendrons increases the radius of the dendrimer, resulting in a stronger association with I_3^- and higher open-circuit voltage with an increasing number of generations. Complexation with $SnCl_2$ reduces the resistance of TPA-DPA and improves the fill factor. The energy conversion efficiency of the DSSC prepared using fifth-generation TPA-DPA is 21% higher than that for the bare film and, when complexed with $SnCl_2$, provides a 34% improvement.

Introduction

Dye-sensitized solar cells (DSSCs)[1] are an attractive, low-cost type of solar cell offering high conversion performance. In 1993, Grätzel et al. reported a DSSC capable of 10% energy conversion efficiency.[2] However, in the 10 years since that report, the efficiency of DSSCs has only been improved by 1%,[3] suggesting that the energy conversion efficiency of these devices has reached a practical limit. Nevertheless, the theoretical energy conversion efficiency of DSSCs is 15% at an open-circuit voltage of 0.9 V,[4] suggesting that further improvements in efficiency should be possible if a suitable breakthrough can be made.

DSSCs are fabricated from nanoporous TiO_2 film, which is impregnated with a dye, a redox electrolyte such as the I^-/I_3^- redox couple, and a counter electrode such as Pt. Following photoexcitation of the sensitized dye, electrons from the excited dye are injected into the TiO_2 conduction band at a velocity of 10^{10-12} s^{-1}. This recombination occurs 100 times slower than reduction of the oxidized dye by I^- (10^6 s^{-1} vs 10^8 s^{-1}). Charge separation in DSSCs is comparable to that of photosynthesis in nature.[5]

At the semiconductor−electrolyte interface, however, the dark current increases exponentially with semiconductor voltage, describing the rectification characteristics of a P−N junction according to Shockley's law.[6] This back electron transfer (from the TiO_2 conduction band to I_3^-) restricts the open-circuit voltage and thus conversion efficiency. Separating the semiconductor and electrolyte is effective for improving the open-circuit voltage but has the effect of retarding the reduction of the oxidized dye.[7]

Triarylamine derivatives have an important place in DSSC research as molecules with multiple functions, most notably electron donation when linked with a sensitized dye and hole transport. Extension of the dye linker stabilizes the charge separation state but delays electron donation.[8] For example, N845 dye adsorbed on TiO_2 film exhibits a remarkably long-lived charge-separated state, with a decay half-time of 0.7 s.[9] Hole-transport derivatives having a spirobifluorene moiety have

(1) (a) Oregan, B.; Grätzel, M. *Nature* **1991**, *353*, 737. (b) Palomares, E.; Clifford, J. N.; Haque, S. A.; Lutz, T.; Durrant, J. R. *J. Am. Chem. Soc.* **2003**, *125*, 475. (c) Adachi, M.; Murata, Y.; Takao, J.; Jiu, J.; Sakamoto, M.; Wang, F. *J. Am. Chem. Soc.* **2004**, *126*, 14943. (d) Horiuchi, T.; Miura, H.; Sumioka, K.; Uchida S. *J. Am. Chem. Soc.* **2004**, *126*, 12218. (e) Dürr, M.; Bamedi, A.; Yasuda, A.; Nellesa, G. *Appl. Phys. Lett.* **2004**, *84*, 3397.
(2) (a) Nazeeruddin, M. K.; Kay, A.; Rodicio, I.; Humphry-Baker, R.; Müller, E.; Liska, P.; Vlachopoulos, N.; Grätzel, M. *J. Am. Chem. Soc.* **1993**, *115*, 6382. (b) Nazeeruddin, M. K.; Péchy, P.; Renouard, T.; Zakeeruddin, S. M.; Humphry-Baker, R.; Comte, P.; Liska, P.; Cevey, L.; Costa, E.; Shklover, V.; Spiccia, L.; Deacon, G. B.; Bignozzi, C. A.; Grätzel, M. *J. Am. Chem. Soc.* **2001**, *123*, 1613.
(3) Grätzel, M. *J. Photochem. Photobiol., A* **2004**, *164*, 3.
(4) Grätzel, M. *J. Photochem. Photobiol., C* **2003**, *4*, 145.
(5) Hagfeldt, A.; Grätzel, M. *Chem. Rev.* **1995**, *95*, 49.
(6) Matsumoto, M.; Wada, Y.; Kitamura, T.; Shigaki, K.; Inoue, T.; Ikeda, M.; Yanagida, S. *Bull. Chem. Soc. Jpn.* **2001**, *74*, 387.
(7) (a) Ferber, J.; Stangl, R.; Luther, J. *Sol. Energy Mater. Sol. Cells* **1998**, *53*, 29. (b) He, J.; Benkö, G.; Korodi, F.; Polívka, T.; Lomoth, R.; Akermark, B.; Sun, L.; Hagfeldt, A.; Sundström, V. *J. Am. Chem. Soc.* **2002**, *124*, 4922. (c) Kusama, H.; Konishi, Y.; Sugihara, H.; Arakawa, H. *Sol. Energy Mater. Sol. Cells* **2003**, *80*, 167.
(8) Bonhôte, P.; Moser, J.-E.; Humphry-Baker, R.; Vlachopoulos, N.; Zakeeruddin, S. M.; Walder, L.; Grätzel. M. *J. Am. Chem. Soc.* **1999**, *121*, 1324−1336.
(9) Hirata, N.; Lagref, J. J.; Palomares, E. J.; Durrant, J. R.; Nazeeruddin, M. K.; Grätzel, M.; Censo, D. D. *Chem. Eur. J.* **2004**, *10*, 595.

10.1021/ja050765c CCC: $30.25

been used in solid-state DSSCs as a replacement of the liquid electrolyte for practical purposes.[10] To obtain energy from such cells, which also contain a P−N junction, it is essential to supply various additives to promote hole mobility and inhibit back electron transfer.[11]

In an attempt to resolve these disadvantages of DSSCs, our group has investigated triphenylamine with dendric phenylazomethine (TPA-DPA)[12] as a hole-transport unit. TPA-DPA consists of a triphenylamine core surrounded by successive generations of phenylazomethine dendrons, forming a thermostable[13] π-conjugated dendric polymer with a single molecular weight. The branching of phenylazomethine dendrons from the triphenylamine core can be controlled precisely on a layer-by-layer basis. These rigid spherical structures assemble as an ordered packing structure upon casting and are thus suitable for the preparation of homogeneous thin films.[13a] The dense packing structure provides an effective and complete shield for the dye in a DSSC. The nitrogen lone pair of the imines also acts as an excellent ligand for metal chlorides and Rhodamine 6G.[14] It is noteworthy that DPA derivatives exhibit stepwise complexation following the basicity gradient of the imine groups in each shell.[15]

A homogeneous film of hole-transporting TPA-DPA can be readily applied in organic light-emitting diodes (OLEDs) as a hole-transport layer. OLEDs prepared using larger dendrimers display better performance, although the turn-on voltage is higher and current density is lower due to the shell effect.[16] This finding indicates that the shell effect suppresses not hole transport to the luminance layer but electron passage from the luminance layer to the anode. Hole transport through the π-conjugated shell thus appears to be advantageous for charge separation. Complexation with $SnCl_2$ also reduces the resistance in the dendrimer film, which may improve device performance.

These unique structural properties of the TPA-DPA dendrimer are expected to act in DSSCs to suppress back electron transfer and thus improve conversion efficiency. Herein is reported the synthesis, structural properties, and metal-assembly of fifth-generation TPA-DPA and the first fabrication of a DSSC using this dendrimer for charge separation.

Results and Discussion

1. Syntheses and Structures of TPA-DPA. Dendric phenylazomethine (DPA) with a phenyl-based core was synthesized up to the fifth generation by a convergent method via reaction of aromatic ketones with aromatic amines.[17] DPA derivatives were previously synthesized by reaction between DPA dendrons having an aromatic ketone and the aromatic amine compounds.[15,18] The present TPA-DPA dendrimers were synthesized by the introduction of three amino groups into the tris[4-(2-thienyl)-phenyl]amine (TPA)[19] (Scheme 1). The Pd coupling reaction of bromonitrobenzene with TPA was carried out through a combination of lithiation and Zn transmetalation.[20] The resulting nitro-substituted TPA was reduced with $NaBH_2S_3$ (prepared by mixing $NaBH_4$ with S[21]) to obtain TPA-NH_2. This conversion could not be achieved using Sn/HCl in water/methanol due to the insolubility of TPA in this solvent. TPA-DPA forms G1 through G5 were synthesized by reaction of TPA-NH_2 with the G1, G2, G3, G4, and G5 dendrons in the presence of titanium(IV) tetrachloride and 1,4-diazabicyclo-[2.2.2]octane (DABCO). TPA-DPA G1−4 were obtained in over 60 wt % yield, while TPA-DPA G5 was afforded in only 11 wt % yield. The TPA-DPA G5 form appeared to be more crowded than the other forms. The dendrimers were characterized by mass spectroscopy (MS), nuclear magnetic resonance (NMR), infrared (IR) spectroscopy, and elemental analysis. Size-exclusion chromatography (SEC) of TPA-DPA G1−5 showed all forms to be monomolecular (Table 1 and Figure S1).

SEC analysis of the structural properties was performed by a combination of differential viscometry, laser light scattering, and refractive index (RI) detection (triple detector SEC; Viscotek).[22] This analysis confirmed that the TPA-DPA molecules were larger than the corresponding DPAs in THF solution. For example, the measured radii of TPA-DPA G5 and DPA G5 were 2.48 and 2.18 nm, respectively.[23] The hydrodynamic radii increased in proportion to the number of generations of the dendrimer structure. The intercepts of this relationship indicate the sizes of the TPA core and the phenyl-based core (Figure 1a).

The intrinsic viscosity ($[\eta]$) is closely related to the molecular structure. Figure 1b shows Mark−Houwink plots ($[\eta] = KM^a$) of the TPA-DPAs and corresponding DPAs. In linear polymers, $[\eta]$ increases continuously with molecular weight (M). However, the present plots display a plateau for higher generations such as G4 and G3. The slopes (a) of the plots in these plateau regions are close to zero, indicating that these dendrimers have a rigid spherical structure similar to a globular protein.[24] The more spherical shape of the TPA-DPA in comparison with DPA is expected considering the trifunctional core of the TPA dendrimer. However, $[\eta]$ for TPA-DPA G5 is lower than that for the smaller dendrimers among the DPA derivatives. The intrinsic viscosity of the dendrimer, expressed as a volume per unit mass ($X^3/2^X$, where X is the generation number), reaches a maximum at the fourth generation,[25] suggesting that the density of TPA-DPA is higher in the fifth generation.

(10) Bach, U.; Lupo, D.; Comte, P.; Moser, J. E.; Weissörtel, F.; Salbeck, J.; Spreitzer H.; Grätzel. M. *Nature* **1998**, *395*, 583.
(11) (a) Krüger, J.; Plass, R.; Cevey, L.; Piccirelli, M.; Grätzel, M. *Appl. Phys. Lett.* **2001**, *79*, 2085. (b) Krüger, J.; Plass, R.; Grätzel. M. *Appl. Phys. Lett.* **2003**, *81*, 367.
(12) Satoh, N.; Cho, J.-S.; Higuchi, M.; Yamamoto, K. *J. Am. Chem. Soc.* **2003**, *125*, 8104.
(13) For reported thermostablity of DPA derivatives, see the following: (a) Higuchi, M.; Shiki, S.; Ariga, K.; Yamamoto, K. *J. Am. Chem. Soc.* **2001**, *123*, 4414. (b) Tanaka, R.; Imaoka, T.; Yamamoto K. *J. Photopolym. Sci. Technol.* **2004**, *17*, 323.
(14) (a) Yamamoto, K.; Higuchi, M.; Shiki, S.; Tsuruta, M.; Chiba, H. *Nature* **2002**, *415*, 509. (b) Nakajima, R.; Tsuruta, T.; Higuchi, M.; Yamamoto, K. *J. Am. Chem. Soc.* **2004**, *126*, 1630. (c) Satoh, N.; Watanabe, T.; Iketaki, Y.; Omatsu, T.; Fujii, M.; Yamamoto, K. *Polym. Adv. Technol.* **2004**, *15*, 159.
(15) (a) Imaoka, T.; Horiguchi, H.; Yamamoto, K. *J. Am. Chem. Soc.* **2003**, *125*, 340. (b) Higuchi, M.; Tsuruta, T.; Chiba, H.; Shiki, S.; Yamamoto, K. *J. Am. Chem. Soc.* **2003**, *125*, 9988.
(16) Satoh, N.; Cho, J.-S.; Higuchi, M.; Yamamoto, K. *J. Photopolym. Sci. Technol.* **2005**, *18*, 55.
(17) (a) Higuchi, M.; Shiki, S.; Yamamoto, K. *Org. Lett.* **2000**, *2*, 3079. (b) Takanashi, K.; Chiba, H.; Higuchi, M.; Yamamoto K. *Org. Lett.* **2004**, *6*, 1709.
(18) Enoki, O.; Imaoka, T.; Yamamoto, K. *Org. Lett.* **2003**, *5*, 2547.
(19) Yamamoto, K.; Higuchi, M.; Uchida, K.; Kojima, Y. *Macromol. Rapid Commun.* **2001**, *22*, 266.
(20) Dong, Y.; Ali, G.; Luping, Y. *J. Am. Chem. Soc.* **1995**, *119*, 11680.
(21) (a) Lalancette, J. M.; Freche, A. *Can. J. Chem.* **1969**, *47*, 739. (b) Lalancette, J. M.; Freche, A. *Can. J. Chem.* **1970**, *48*, 2366.
(22) (a) Yau, W. W.; Rementer S. W. *J. Liq. Chromatogr.* **1990**, *13*, 627. (b) Jackson, C.; Yau, W. W. *J. Chromatogr.* **1993**, *645*, 209. (c) Jackson, C.; Yau, W. W. *Adv. Chem. Ser.* **1995**, *247*, 69.
(23) (a) Ihre, H.; Hult, A.; Söderlind, H. *J. Am. Chem. Soc.* **1996**, *118*, 6388. (b) Cardona, C. M.; Kaifer, A. E. *J. Am. Chem. Soc.* **1998**, *120*, 4023.
(24) Tomalia, D. A.; Naylor, A. M.; Goddard, W. A., III. *Angew. Chem., Int. Ed. Engl.* **1990**, *29*, 138.

Scheme 1. Synthesis of TPA-DPA G1−5

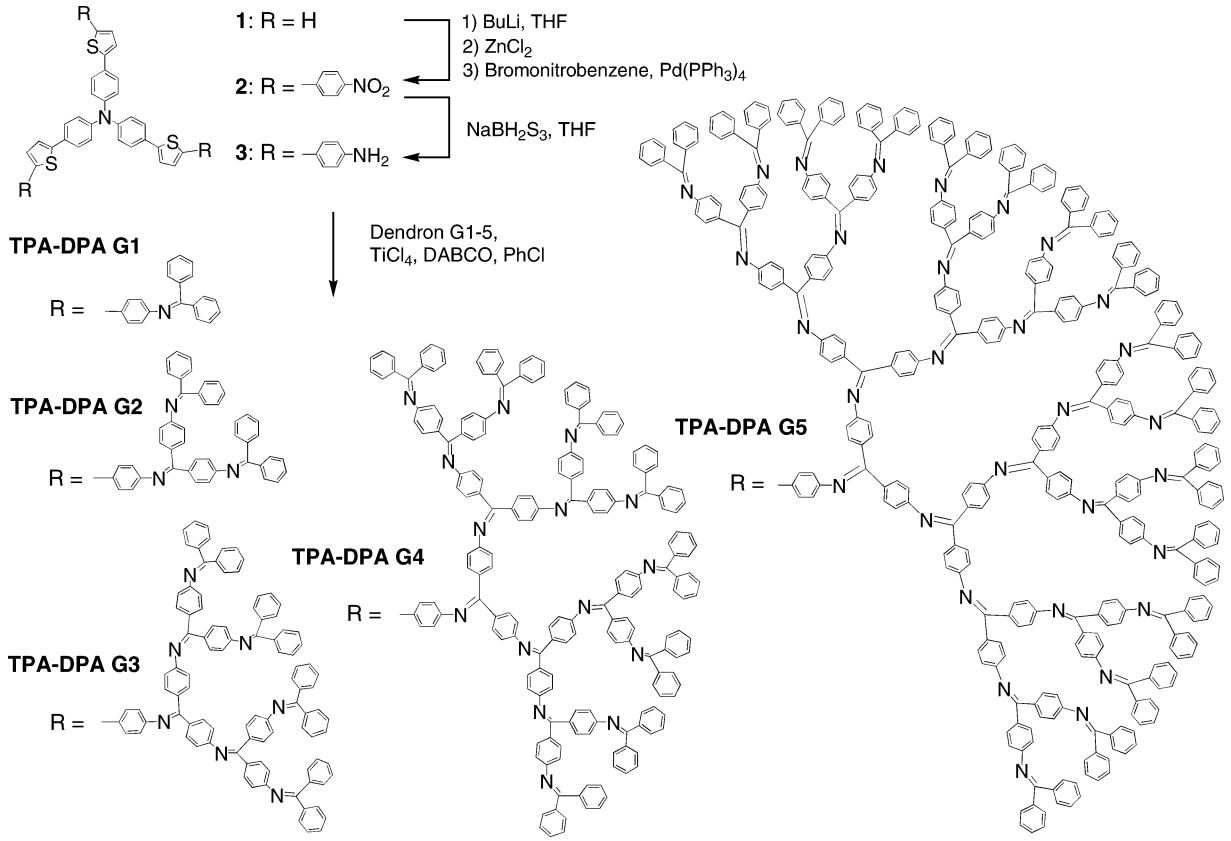

Table 1. Physicochemical Characteristics of TPA-DPAs

TPA-DPA	M_{calcd}	MALDI-TOF mass	yield (%)	Tri-SEC M_w/M_n	Tri-SEC log{[η] (dL/g)}	Tri-SEC R_h (nm)	CV $E_{1/2}$ (V vs Fc/Fc$^+$)	CV ln[k_{ET} (cm/s)]
G1	1257.63	1257.6	94	1.01	−1.29	0.96	0.379	−1.71
G2	2332.94	2332.4	74	1.01	−1.15	1.35	0.381	−3.03
G3	4483.54	4483.1	69	1.01	−1.13	1.69	0.367	−3.87
G4	8784.76	8782.7	67	1.01	−1.11	2.11	0.375	−5.91
G5	17387.18	17393.3	11	1.02	−1.23	2.43	0.378	−6.72

The intercepts (log$K$) of the Mark−Houwink plots, which correspond to the density of the polymers, show that the densities of TPA-DPA G1−4 are lower than those of DPA G1−5. This result is consistent with the observation that the radius of TPA-DPA is larger than that of DPA. Thus, TPA-DPA generally has a larger core and central space[26] than the corresponding DPA. However, the plot of TPA-DPA G5 falls on the same line as DPA G3−5, that is, TPA-DPA G5 is just as crowded as the DPAs, although it has a larger core. The dendrons of TPA-DPA G5 may therefore extend into the central space, or be more tightly packed. The increased density of TPA-DPA G5 is also in good agreement with its lower yield (11 wt %).

The results of SEC structural analysis were verified by electrochemical analysis. The shell effect was observed in the cyclic voltammograms of the dendrimers,[15(a),27] where the TPA unit of the core produced a redox wave of the N/N$^{+\bullet}$ couple at around 0.4 V vs Fc/Fc$^+$. This redox wave broadened as the generation number increased (Figure S2). As the diffusion coefficients (4.92×10^6 and 1.94×10^6 cm^2 s^{-1} for TPA-DPA G1 and G5, respectively) calculated from the hydrodynamic radii are of the same order as the electron-transfer rate, these broad waves are considered to be caused not by a decrease in the diffusion coefficient but by a change in the rate of electron transfer due to separation of the core from the electrolyte by the dendric shells.

The electron-transfer rate constant (k_{ET}) decays exponentially with distance (R), as given by $k_{ET} \approx \exp(-\beta R)$. The attenuation factor (β) indicates the barrier height of the intervening medium and typically varies from 0.2 to 1.4 Å^{-1}.[28,29] The values of k_{ET}

(25) (a) Mourey, T. H.; Turner, S. R.; Rubinstein, M.; Fréchet, J. M. J.; Hawler, C. *Macromolecules* **1992**, *25*, 2401. (b) de Brabander-van den Berg, E. M. M.; Meijer, E. W. *Angew. Chem., Int. Ed. Engl.* **1993**, *32*, 1308. (c) Naylor, A. M.; Goddard, W. A., III; Keifer, G. E.; Tomalia, D. A. *J. Am. Chem. Soc.* **1989**, *111*, 2339.

(26) From Figure 1a, the radius of the TPA core and the phenyl-based core is estimated to be 5.80 and 2.15 Å, respectively. Regarding the central space as a sphere, this space in the TPA-DPAs and DPAs is calculated to be 817 Å^3 and 41.6 Å^3, respectively. Thus, the space in TPA-DPAs is 20 times that of DPAs.

(27) (a) Matos, M. S.; Hofkens, J.; Verheijen, W.; De Schryver, F. C.; Hecht, S.; Pollak, K. W.; Fréchet, J. M. J.; Forier, B.; Dehaen, W. *Macromolecules* **2000**, *33*, 2967. (b) Tomoyose, Y.; Jiang, D.-L.; Jin, R.-H.; Aida, T.; Yamashita, T.; Horie, K.; Yashima, E.; Okamoto, Y. *Macromolecules* **1996**, *29*, 5236. (c) Goman, C. B.; Smith, J. C.; Hager, M. W.; Parkhurst, B. L.; Sierzputowska-Gracz, H.; Haney, C. A. *J. Am. Chem. Soc.* **1999**, *122*, 9958.

(28) (a) Kelley, S. O.; Barton, J. K. *Science* **1999**, *283*, 375. (b) Tolbert, L. M. *Acc. Chem. Res.* **1992**, *25*, 561.

(29) (a) Winkler, J. R.; Gray, H. B. *Chem. Rev.* **1992**, *92*, 369. (b) Moser, C. C.; Kseske, J. M.; Warncke, K.; Farid, R. S.; Dutton, P. L. *Nature* **1992**, *355*, 796.

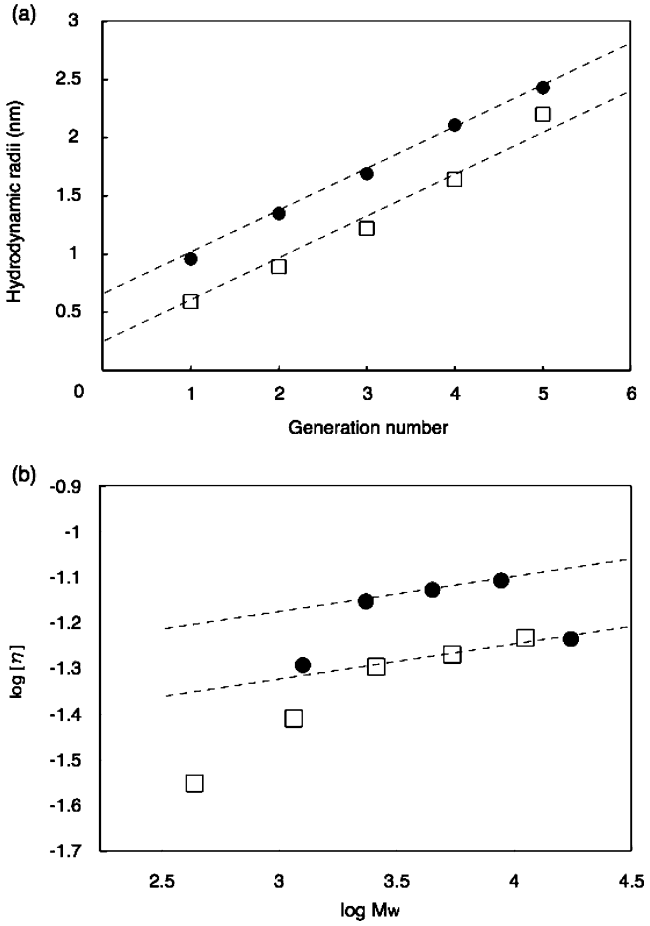

Figure 1. (a) Hydrodynamic radii as a function of generation number, and (b) Mark−Houwink plot of DPA (squares) and TPA-DPA(circles)

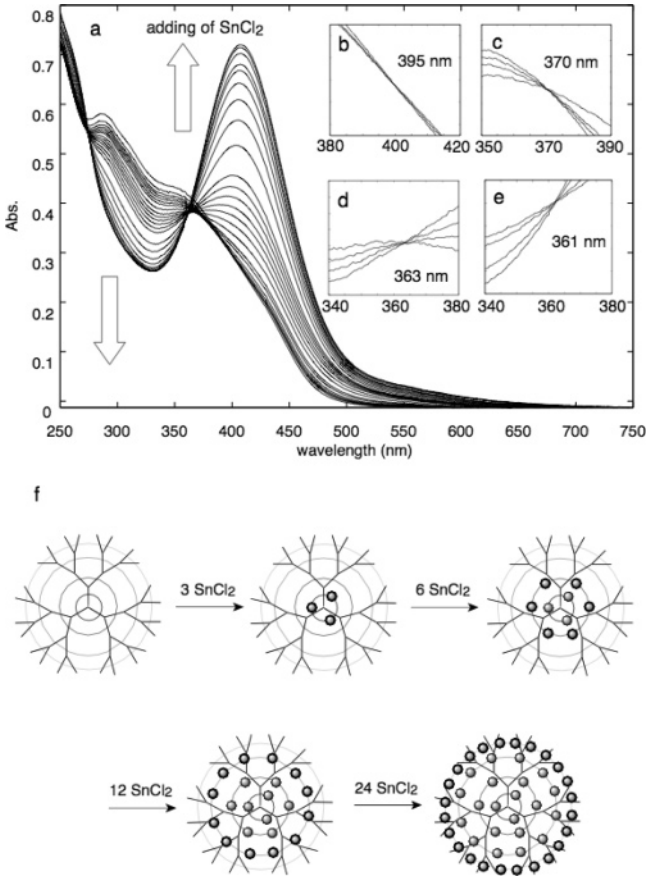

Figure 2. UV−vis spectra of TPA-DPA G4 complexed with (a) 0−45, (b) 0−3, (c) 4−9, (d) 10−21, and (e) 22−45 equiv of $SnCl_2$ (solvent 1:1 dichloromethane/acetonitrile), and (f) schematic representation of stepwise radial complexation of TPA-DPA G4 with $SnCl_2$.

for core redox in TPA-DPA G1−G5, determined from the peak separations at various scan rates, display a dependence on the hydrodynamic radius (Figure S3). The value of β obtained from this relationship, 0.35, is typical for electron transfer through π-conjugated spacers.[30] These results support the notion that the dendric shells grow radially from the TPA core to form a spherical structure.

Such a low value of β is expected to be beneficial for long-range charge transfer[31] from the TPA core to the oxidized dye through the dendric shells.[32] The long-range electron transfer through the π-conjugated bridge requires mixing between the bridge and the donor electronic level.[33] The redox potential of the TPA core, an electron donor, is close to the oxidation potential of the π-conjugated DPA as a bridge. Based on the mismatch of electronic levels, it can be safely assumed that this bridge does not participate in back electron transfer from the TiO_2 conduction band to the I_3^- or the TPA (Figure S4). As a result, the value of β in this back electron transfer is assumed to be ca. 1.6, which has previously been observed for N845 dye adsorbed on TiO_2 film.[9] The difference in β values varies exponentially with differences in electron-transfer kinetics associated with the division between donors and acceptors. If the acceptor in the back electron transfer (I_3^-) is not present in TPA-DPA, an increase in the dendrimer radius would inhibit back electron transfer relative to regeneration of the dye in a DSSC.

2. Controlled Metal-Assembling Functionality of TPA-DPA. The metal-assembling property of TPA-DPA was confirmed by spectroscopic measurements. Upon addition of $SnCl_2$, TPA-DPA G4 exhibited a complexation behavior similar to that of DPA G4.[14a] Using ultraviolet−visible (UV−vis) spectroscopy to monitor the titration of $SnCl_2$ to an equimolar level (per binding site, 45 equiv), four changes in the position of the isosbestic point were observed, indicating that the complexation proceeds not randomly but stepwise (Figure 2). The appearance of these four isosbestic points suggests that four different complexes are formed successively upon $SnCl_2$ addition.

The absorption band near 400 nm attributable to this complexation strengthens with the addition of $SnCl_2$, accompanied by a weakening of the absorption bands near 320 nm attributable

(30) (a) Helms, A.; Heiler, D.; McLendon, G. *J. Am. Chem. Soc.* **1992**, *114*, 6227. (b) Tour, J. M. *Chem. Rev.* **1996**, *96*, 537.
(31) Davis, W. D.; Svec, W. A.; Ratner, M. A.; Wasielewski, M. R. *Nature* **1998**, *396*, 60.
(32) The electron transfer from TPA-DPAs to the oxidized dye was confirmed in nanosecond laser transient absorbance measurements, using the N719-sensitzed TiO_2 films and TPA-DPA G1. In the absence of TPA-DPA G1, dye breaching around 500 nm is observed. Covered with TPA-DPA G1, the reduction of this oxidized dye occurred within 10^{-8} s, and the formation of the TPA cation was shown by the rise in the absorption around 600 nm. Under the same condition, the lifetime of this cation (20 μs) was observed to be twice that of the oxidized dye (10 μs) in the absence of TPA-DPA G1. On the other hand, the electron transfer from I^- to the TPA cation was observed by the following method: We chemically oxidized TPA-DPA G1 with $NOBF_4$ to obtain a broad absorption around 1100 nm; this absorption immediately disappeared on addition of I^-. This result suggests the occurrence of charge transfer between the TPA core and I^-.
(33) Pourtois, G.; Beljonne, D.; Cornil, J.; Ratner, M. A.; Brédas, J. L. *J. Am. Chem. Soc.* **2002**, *124*, 4436.

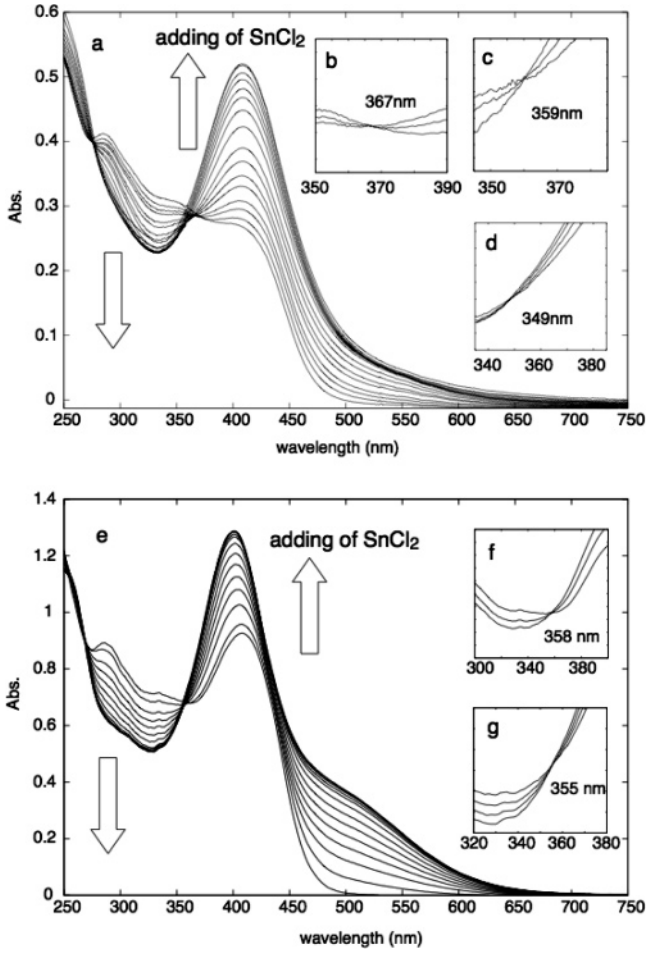

Figure 3. UV−vis spectra of TPA-DPA G3 complexed with (a) 0−21, (b) 0−3, (c) 4−9, and (d) 10−21 equiv of $SnCl_2$ and of TPA-DPA G2 complexed with (e) 0−9, (f) 0−3, and (g) 4−9 equiv of $SnCl_2$ (solvent 1:1 dichloromethane/acetonitrile).

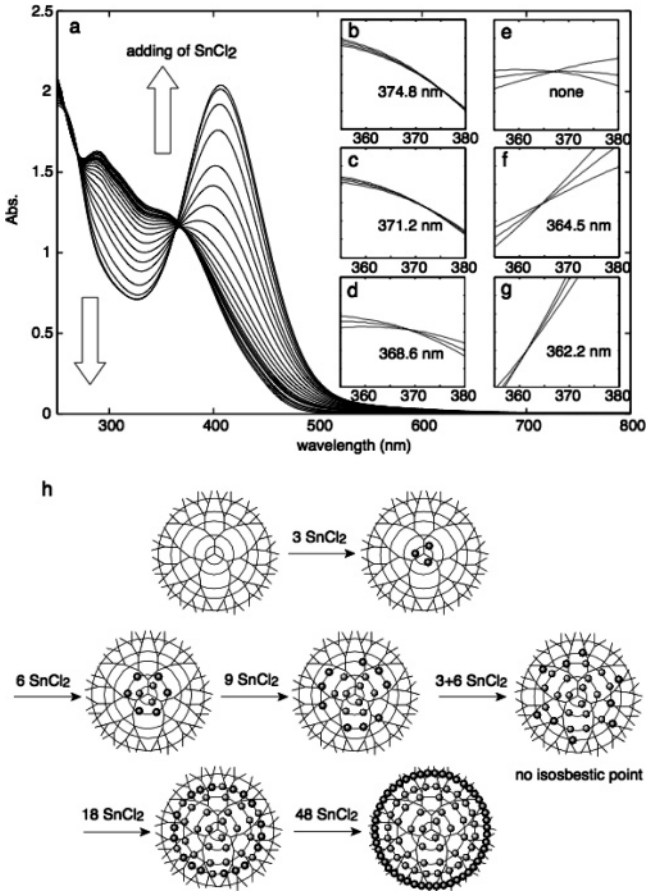

Figure 4. UV-vis spectra of TPA-DPA G5 complexed with (a) 0−93, (b) 0−3, (c) 4.5−9, (d) 12−18, (e) 18−27, (f) 33−45, and (g) 45−93 equiv of $SnCl_2$ (solvent 1:1 chloroform/acetonitrile), and (h) schematic representation of stepwise radial complexation of TPA-DPA G5 with $SnCl_2$

to the phenylazomethine unit (Figure 2a). The spectra of TPA-DPA G4 changed gradually with the addition of $SnCl_2$ up to 3 equiv, exhibiting an isosbestic point at 395 nm (Figure 2b). The isosbestic point shifted upon further addition of $SnCl_2$ to 370 nm at 3−9 equiv (Figure 2c), 363 nm at 10−21 equiv (Figure 2d), and 361 nm at 22−45 equiv (Figure 2e). Overall, the number of equivalents of $SnCl_2$ required to induce a shift was consistent with the number of imine sites present in the successive layers of TPA-DPA G4. These titration results suggest that the complexation proceeds in a stepwise fashion from the core imines to the terminal imines of TPA-DPA G4 (Figure 2f).

A similar stepwise complexation was observed for TPA-DPA G3 and TPA-DPA G2 (Figure 3). TPA-DPA G3 exhibited three isosbestic points, at 367, 360, and 355 nm upon addition of 0−3, 4−9, and 10−21 equiv of $SnCl_2$, respectively (Figure 3a−d), while TPA-DPA G2 displayed two isosbestic points, at 344 and 355 nm for 0−3 and 4−9 equiv, respectively (Figure 3e-g). Again, the number of equivalents of $SnCl_2$ required to shift the isosbestic points is consistent with the number of imine sites present in each layer of the dendrimers. The added $SnCl_2$ thus appears to be incorporated in a stepwise fashion by successively filling layers outward from the TPA core. The imine group in the DPA acts as an excellent coordination site with Lewis acids due to its strong basicity. The stepwise coordination of $SnCl_2$ is thus considered to be driven by an increase in the inner imine basicity.

The complexation sequence for TPA-DPA G5 also proceeds in a stepwise fashion, but in this case the fourth layer is filled before complexation of the third layer is complete. The five isosbestic points appeared at 375, 371, 369, 365, and 362 nm upon addition of 0−3, 4.5−9, 12−18, 33−45, and 45−93 equiv of $SnCl_2$ (Figure 4b−d, f, g). No isosbestic point appeared upon addition of 18−27 equiv of $SnCl_2$ (Figure 4e), suggesting that at least two types of complexation occurred in this case. In comparison with the number of imines in each layer, the number of equivalents of $SnCl_2$ required for each step suggests the following sequence of metal assembly in TPA-DPA G5: the first and second layers are fully filled by 3 and 6 equiv of $SnCl_2$, the third layer is filled with 9 equiv, three imines left open in the third layer and six imines in the fourth layer (no isosbestic point was observed here) complex with 9 equiv simultaneously, and finally the empty fourth and fifth layers are filled by 18 and 48 equiv (Figure 4h). Stepwise metal assembly in the DPA derivatives occurs due to the difference in imine basicity with the next layer. In the case of TPA-DPA G5, the difference in basicity between the third and fourth layers is smaller than that between the other layers, apparently as a feature of the growth of π-conjugation. This produces a typical environment (i.e., electron donation) for polymer chains.[34] Nevertheless, the existence of five isosbestic points indicates stepwise metal assembly in TPA-DPA G5,[35] suggesting that this form has the

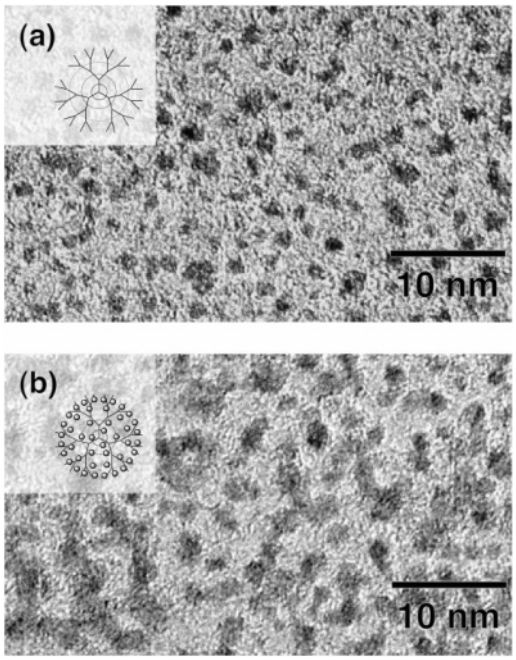

Figure 5. TEM images of (a) TPA-DPA G4 and (b) $(SnCl_2)_{45}$@TPA-DPA.

largest number of strong coordination sites among the TPA-DPAs considered in this study.

Metal assembly in the TPA-DPAs was also observed by transmission electron microscopy (TEM) and high-performance particle sizing (HPPS) measurements. TEM images of the solid-state TPA-DPA G4 and $(SnCl_2)_{45}$@TPA-DPA G4 (Figure 5) reveal that complexation increases the average particle size from 2.8 nm ($\sigma = 0.53$ nm) to 3.2 nm ($\sigma = 0.64$), suggesting that $SnCl_2$ was incorporated into the TPA-DPA. The average sizes of DPA G4 and $(SnCl_2)_{30}$@DPA G4 are 2.3 and 2.7 nm, respectively. The TPA core is larger than the phenyl core of the DPAs. The HPPS measurements, conducted using a Sysmex particle sizer based on dynamic light scattering, revealed the diameters of TPA-DPA G4 and $(SnCl_2)_{45}$@TPA-DPA G4 to be 4.13 and 5.44 nm, respectively (Figure S5). The particle sizes of TPA-DPA G4 estimated by HPPS and triple-detector SEC are in fair agreement. The time-of-flight (TOF) mass spectrum of TPA-DPA G2 upon addition of 3 equiv of $SnCl_2$ displayed a molecular peak at 2901.7 based on $(SnCl_2)_3$@TPA-DPA G2 (calcd 2901.8) and fragment peaks for the complex (Figure 6). This result suggests that the complexation of $SnCl_2$ with imine groups proceeds without separation of Cl^-. The tin(II) atom, with tetrahedral electron pair geometry,[36] is surrounded by two chlorine atoms and one nitrogen atom of the imine group. These results also support the incorporation of $SnCl_2$ into the TPA-DPA structure.[37]

Complexation with $SnCl_2$ reduces the resistance of TPA-DPA.[16] The addition of equimolar amounts (per binding site)

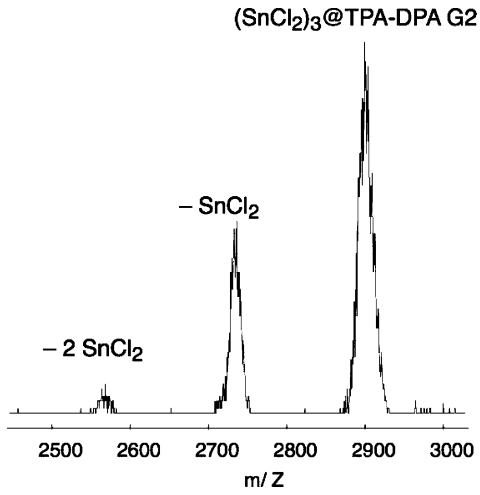

Figure 6. TOF mass spectrum of $(SnCl_2)_3$@TPA-DPA G2 (TPA-DPA G2 with 3 equiv of $SnCl_2$).

of $SnCl_2$ increased the conductivity of the insulating TPA-DPA G3 film to 1.6×10^{-8} S/cm under atmospheric conditions. The cyclic voltammogram of the modified electrode with TPA-DPA G4 and $SnCl_2$@TPA-DPA G4 displays a reversible redox wave (Figure S6). Complexation with 1 equiv of $SnCl_2$ results in a redox potential shift of +17 mV, and the peak potential difference (ΔE_p) decreased from 94 mV to 63 mV. Based on these ΔE_p values, the estimated values of k_{ET} for TPA-DPA G4 and $SnCl_2$@TPA-DPA G4 are 1.0 s^{-1} and 2.3 s^{-1}, respectively. The redox peak in $SnCl_2$@TPA-DPA G4 is twice that in TPA-DPA G4, and the capacitance of $SnCl_2$@TPA-DPA G4 is smaller than that of TPA-DPA G4. These electrochemical observations also suggest that $SnCl_2$ promotes mediation of electron transfer in the dendrimer as a result of the reduced resistance.

3. Photovoltaic Performance of DSSC Using TPA-DPA. Control of the semiconductor/dye/electrolyte interface is important in the improvement of solar cell performance, as it is at this interface that the photoinduced primary reaction steps occur in DSSCs. To investigate the performance of TPA-DPA experimentally, layers of TPA-DPA G1−5 were spun using 1 g/L chlorobenzene solution onto nanoporous TiO_2 film (ca. 10 μm) coated with Ru dye (N719). For photovoltaic measurements, the space between the TiO_2 film and the Pt counter electrode was filled with an electrolyte composed of 0.6 M dimethylpropylimidazolium iodide (DMP II), 0.05 M iodine, and 0.1 M lithium iodide in 3-methoxypropionitrile (MPN). The current−voltage characteristics were obtained at an illumination intensity of 1 sun (global AM 1.5, 100 mW/cm^2).[38]

The performance characteristics of the tested cells are summarized in Table 2. Open circuit voltage (V_{oc}) of the

(34) The estimation of the complexation constants, *K*, in each layer of the Half-DPAs has been reported. The *K* of the first, second, and end layers is almost the same as that between G3 and G4. Thus, we can assume that the *K* of the first, second, and end layer in TPA-DPA G5 is almost the same as that in TPA-DPA G3 and G4. In other words, the difference in the *K* between the third and fourth layer becomes small in TPA-DPA G5. For a discussion on the physical basis for isosbestic point shifts in the Half-DPAs, see the following: Yamamoto, K.; Higuchi, M.; Kimoto, A.; Imaoka, T.; Masachika, K. *Bull. Chem. Soc. Jpn.* **2005**, *78*, 349.

(35) In the crowded structure of TPA-DPA G5, a longer time is required until the complexation with the first layer imines is finished.

(36) (a) Kokunov, Y. V.; Detkov, D. G.; Gorbunova, Y. E.; Ershova, M. M.; Mikhailov, Y. N. *Russ. J. Coord. Chem.* **2002**, *26*, 857. (b) Tang, Y.; Felix, A. M.; Zakharov, L. N.; Rheingold, A. L.; Kemp, R. A. *Inorg. Chem.* **2004**, *43*, 7239.

(37) For reported metal-assembling in other dendrimers, see the following. (a) Petrucci-Samija, M.; Guillemette, V.; Dasgupta, M.; Kakkar, A. K. *J. Am. Chem. Soc.* **1999**, *121*, 1968. (b) Balogh, L.; Tomalia, D. A. *J. Am. Chem. Soc.* **1998**, *120*, 7355. (c) Zhao, M.; Sun, L.; Crooks, R. M. *J. Am. Chem. Soc.* **1998**, *120*, 4877. (d) Ispasoiu, R. G.; Balogh, L.; Varnavski, O. P.; Tomalia, D. A.; Goodson, T., III. *J. Am. Chem. Soc.* **2000**, *122*, 11005. (e) Varnavski, O.; Ispasoiu, R. G.; Balogh, L.; Tomalia, D.; Goodson, T., III. *J. Chem. Phys.* **2001**, *114*, 1962. (f) Scott, R. W. J.; Datye, A. K.; Crooks, R. M. *J. Am. Chem. Soc.* **2003**, *125*, 3708. (g) Zheng, J.; Petty, J. T.; Dickson, R. M. *J. Am. Chem. Soc.* **2003**, *125*, 7780. (h) Lang, H.; May, A. M.; Iversen, B. L.; Chandler, B. D. *J. Am. Chem. Soc.* **2003**, *125*, 14832.

(38) The spectral overlap of AM 1.5 G solar emission with our simulated AM 1.5 G light emission is shown in Figure S7.

Table 2. Performance of DSSCs Using TPA-DPA

treatment	J_{sc} (mA/cm^2)	V_{oc} (mV)	*ff*	*Ef*[a] (%)
none	14.5	694	0.58	5.84
TPA-DPA G1	13.3	727	0.63	6.12
TPA-DPA G2	12.9	770	0.62	6.17
TPA-DPA G3	13.6	789	0.58	6.32
TPA-DPA G4	13.1	816	0.60	6.44
TPA-DPA G5	13.7	833	0.59	6.74

[a] Irradiance, 100 mW/cm^2 (AM 1.5G); illuminated area, 0.24 cm^2; electrolyte, 0.6 M DMP II, 0.05 M I_2, 0.1 M LiI in MPN. J_{sc}: short circuit current density. V_{oc}: open circuit voltage. *ff*: fill factor. *Ef*: energy conversion efficiency.

DSSCs increased with the generation number of the TPA-DPA, whereas short circuit current density (J_{sc}) was lower for all cells containing TPA-DPA compared to the as-prepared TiO_2/N719 surface. TPA-DPA G1−2 provided improved fill factors (*ff*), whereas TPA-DPA G3−5 offered little or no improvement. The increase in V_{oc} is due to a decrease in back electron transfer at the semiconductor-electrolyte interface.[39] Dark current arises from the reduction of triiodide by conduction band electrons ($I_3^- + 2\ e^- \rightarrow 3\ I^-$) and may be influenced by the presence of TPA-DPA.

I^-/I_3^- and I_3^-/I_2 redoxes were observed in the cyclic voltammogram of the I^- solution: $6\ I^- \leftrightarrow 2\ I_3^- + 4\ e^- \leftrightarrow 3\ I_2 + 6\ e^-$ (Figure S8). The I^-/I_3^- redox couple was significantly affected by treatment of the electrode with TPA-DPA G3 and G4, while the I_3^-/I_2 redox was not affected. In particular, the larger TPA-DPA G4 exhibited lower current of triiodide reduction, supporting the notion that the presence of TPA-DPA increases V_{oc} due to inhibition of back electron transfer from the TiO_2 interface. The I^-/I_3^- redox is consider to be irreversible, as I_3^- associates with imines on the TPA-DPA.

The association between I_3^- and imines was confirmed by UV−vis spectroscopy, which showed a weakening of the absorbance due to I_3^- upon addition of phenylazomethine.[40] The Job plot[41] shows a minimum at a 0.33 molar fraction of I_3^-, indicating that phenylazomethine forms a 1:2 complex with I_3^- similar to pyridines (Figure S9).[42] This reaction reduces the I_3^- concentration and increases the I^- concentration. The concentration of I_3^- decreases more sensitively in the larger TPA-DPAs as a result of the stepwise radial complexation of coordinate sites starting from the strongest sites close to the core, which associates with I_3^- more strongly. The growth of dendrimers maintains a separation between the TiO_2 surface and I_3^- or the TPA core. On the basis of the β discussion, these two processes contribute to the improvement of V_{oc}. The dependence of V_{oc} on the I_3^- concentration is also indicated in regenerative photoelectrochemical systems.[39c,43]

Treatment of the dye-adsorbed surface with TPA-DPA prevents the decay of J_{sc} in the longer term. The dendrimers thus protect the dye from denaturants that may form through thiocyanato ligand exchange.[44] The shell effects of the TPA-DPA also contribute to long-term stability in DSSCs.

The lower values of *ff* in the DSSC prepared with larger TPA-DPAs are considered to be due to the increased resistance of the dendrimer layers.[6,7a] Complexation with $SnCl_2$ is thus expected to improve cell performance by reducing the resistance of the TPA-DPA. Figure 7 shows the current−voltage (*I*−*V*) curves of the as-prepared DSSC, a DSSC coated with TPA-DPA G5, a DSSC coated with $SnCl_2$@TPA-DPA G5, and a DSSC coated with 0.5 M *t*-BuPy. The as-prepared DSSC exhibits a performance of $J_{sc} = 14.4$ mA/cm^2, $V_{oc} = 0.68$ V, and $ff = 0.53$, corresponding to $Ef = 5.21\%$. On treatment with TPA-DPA G5, V_{oc} increased to 0.81 V, *ff* increased to 0.58, and *Ef* was raised to 6.45%, while J_{sc} was lowered to 13.6 mA/cm^2.[45] The complex of TPA-DPA G5 with $SnCl_2$ provided a further improvement in *ff* to 0.65, with a corresponding *Ef* of 7.12%.

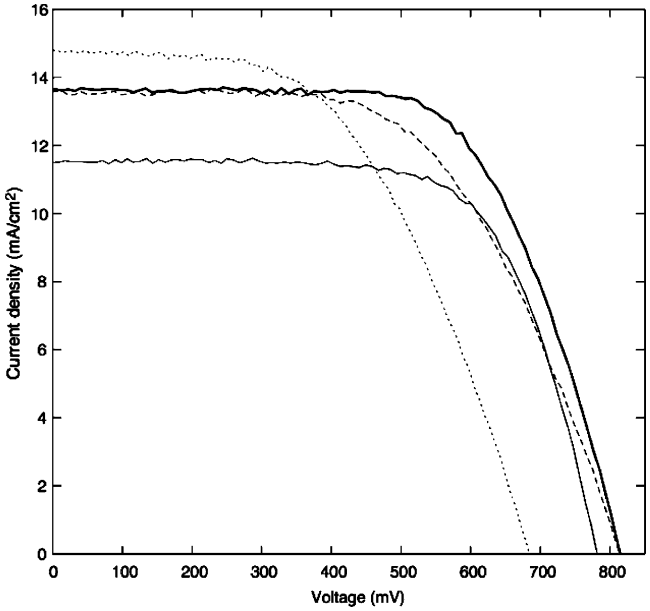

Figure 7. Photocurrent density and voltage characteristics of DSSCs prepared with $SnCl_2$@TPA-DPA G5 (bold solid line), TPA-DPA G5 (dashed line), and *t*-BuPy (thin solid line) for comparison with the as-prepared device (dotted line). Irradiance: 100 mW/cm^2 (simulating AM 1.5G). Illuminated area: 0.25 cm^2. Film thickness: 10 μm. Electrolyte: 0.6 M DMP II, 0.05 M I_2, 0.1 M LiI in MPN.

This improvement in *ff* is supported by the electrochemical results (Figure S10). The electrode treated with $SnCl_2$@TPA-DPA G4 produced a higher current of I^- oxidation without appreciable effect on I_3^- reduction in comparison to the TPA-DPA G4 cell. Although complexation with $SnCl_2$ promotes electron transfer from I^- to the electrode through the TPA-DPA, 1 equiv of $SnCl_2$ does not block the association between I_3^- and phenylazomethine. This result suggests that complexation with $SnCl_2$ reduces the dendrimer resistance, thereby smoothing the dye regeneration reaction ($6\ I^- \rightarrow 2\ I_3^- + 4\ e^-$).

In comparison with the as-prepared DSSC, treatment with TPA-DPA G5 and the $SnCl_2$@TPA-DPA G5 complex increases

(39) (a) Ferber, J.; Stangl, R.; Luther, J. *Sol. Energy Mater. Sol. Cells* **1998**, *53*, 29. (b) Palomares, E.; Clifford, J. N.; Haque, S. A.; Lutz, T.; Durrant, J. R. *J. Am. Chem. Soc.* **2003**, *125*, 475. (c) Huang, S. Y.; Schlichthörl, G.; Nozik, A. J.; Grätzel, M.; Frank. A. J. *J. Phys. Chem. B* **1997**, *101*, 2576.
(40) Langmuir, M. E.; Parker, M. A.; Rauh, R. D. *J. Electrochem. Soc.* **1982**, *129*, 1705.
(41) (a) Job, P. *Ann. Chem.* **1928**, *9*, 113. (b) Vosburgh, W. C.; Cooper, R. G. *J. Am. Chem. Soc.* **1941**, *63*, 437. (c) Hill, Z. D.; MacCarthy, P. *J. Chem. Educ.* **1986**, *63*, 162.
(42) (a) Kebede, Z.; Lindquist, S.-E. *Sol. Energy Mater. Sol. Cells* **1999**, *57*, 259. (e) Reid, C.; Mulliken, R. S. *J. Am. Chem. Soc.* **1954**, *76*, 3869. (b) Álvarez-Rúa, C.; García-Granda, S.; Ballesteros, A.; González-Bobes, F.; González, J. *Acta Crystallogr.* **2002**, *E58*, o1381.
(43) (a) Rosenblut, M. L.; Lewis, N. S. *J. Phys. Chem.* **1989**, *93*, 3735. (b) Kumer, A.; Santangelo, P. G.; Lewis, N. S. *J. Phys. Chem.* **1992**, *96*, 835. (c) Huang, S. Y.; Schlichthörl, G.; Nozik, A. J.; Grätzel, M.; Frank, A. J. *J. Phys. Chem. B* **1997**, *101*, 2576.
(44) Greijer, H.; Lindgren, J.; Hagfeldt, A. *J. Phys. Chem. B* **2001**, *105*, 6314.
(45) This value is lower than that of Table 2, because the performance of the DSSC using the dendrimer reflects that of the untreated DSSC.

Ef by 21% and 34%, respectively. The DSSC prepared with *t*-BuPy exhibited a performance of $J_{sc} = 13.0$ mA/cm^2, $V_{oc} = 0.78$ V, $ff = 0.66$, and $Ef = 6.73\%$. The energy conversion efficiency of the DSSC with $SnCl_2$@TPA-DPA G5 therefore exceeds that of the *t*-BuPy reference cell by 15%.

Conclusions

Hole-transporting phenylazomethine dendrimers with a triphenylamine core were synthesized by a convergent method via reaction of aromatic ketones with aromatic amines in the presence of titanium(IV) tetrachloride. The obtained dendrimers exhibit the viscous character of a rigid spherical molecule, with a hydrodynamic radius proportional to the number of generations of dendron growth. Electrochemical analysis revealed that the π-conjugated dendron shells isolate the triphenylamine core at the center of the dendrimer and that the triphenylamine core is oxidized through the dendron shell with an attenuation factor of 0.35. Spectroscopic analysis indicated the complexation between TPA-DPA and $SnCl_2$ occurs stepwise in an outward radial direction following the basicity gradient of imines in each dendric shell. DSSCs prepared using larger TPA-DPAs exhibited higher open-circuit voltage. The increase in radius and association with I_3^- contributes exponentially to the inhibition of back electron transfer based on the difference in β values. This contribution is advantageous for improving V_{oc}, since back electron transfer increases exponentially with voltage. Complexation with $SnCl_2$ reduces the resistance of TPA-DPA for hole transfer through the dendric shells, thereby improving the fill factor.

Experimental Section

Materials. 4,4′-Diaminobenzophenone was purchased from Fluka, and tin(II) chloride was obtained from Wako Pure Chemical Industries. For the fabrication of DSSCs, Ti-Nanoxide T, N719 dye, and DMP II were procured from Solaronix. 3-Methoxypropionitrile was purchased from Aldrich. A fluorine-doped tin oxide (FTO) glass sheet was obtained from Asahi Glass. All other chemicals were purchased from Kantoh Kagaku. $NaBH_2S_3$ was synthesized according to a literature method.[21] Tris[4-(2-thienyl)-phenyl]amine (TPA)[19] and all the DPA dendrons (G2−5)[17] were synthesized according to the previously reported methods.

Analytical Measurements. NMR spectra were recorded using a JEOL JMN400 Fourier transform NMR spectrometer (400 MHz) in $CDCl_3$ (with tetramethylsilane as internal standard) solution. Matrix-Assisted Laser Desorption/Ionization (MALDI) TOF mass spectra were obtained using a Shimadzu/Kratos KOMPACT MALDI mass spectrometer (Positive mode; Matrix, Dithranol). Analytical size-exclusion chromatography (SEC) was performed using an HPLC (Shimadzu, LC-10AP) equipped with a TSK-GEL CMHXL (Tosoh) at 40 °C. Tetrahydrofran (THF) was used as the eluent at a flow rate of 1 mL/min. The detection line was connected to a triple detector (Viscotek, TriSEC Model 302). A 100 μL aliquot of a THF solution of TPA-DPA or DPA (4−5 mg/1 mL) was injected onto a gel column. The cyclic voltammograms were recorded using an ALS 710A electrochemical analyzer with Pt working electrode (polished in advanced with 0.05 mm alumina paste), Pt wire counter electrode, and Ag/Ag$^+$ reference electrode. The potential was referenced to a ferrocene/ferrocenium (+0.550 V vs NHE) base. Nanosecond laser transient absorbance measurements were performed using laser pulses from a Q-switched Nd:YAG Laser (532 nm, Continuum) and a streak camera system consisting of a Hamamatsu Photonics diffraction grating spectroscope (C5094), streak unit (C7700-01), and charge-coupled device (CCD) camera (C4742-98-24NR). For UV−vis spectroscopy, the dye-adsorbed films were coated with ethylene carbonate/propylene carbonate (v/v = 1/1). Spectra were recorded using a Shimadzu UV-3100PC spectrometer with a closed quartz cell (optical path length, 1 cm).

For the observation of radial stepwise complexation, a capped quartz cell was filled with 3 mL of dehydrated chloroform/acetonitrile (v/v = 1/1) solution containing TPA-DPA G2 ($2/3 \times 10^{-5}$ M), TPA-DPA G3 ($1/3 \times 10^{-5}$ M), TPA-DPA G4 ($1/9 \times 10^{-5}$ M), or TPA-DPA G5 (2×10^{-6} M). UV−vis spectra were then recorded while dropping 1 molar equiv per binding site of a 3 μL aliquot of a dehydrated acetonitrile solution of $SnCl_2$ ($2/3 \times 10^{-2}$ M, $1/3 \times 10^{-2}$ M, $1/9 \times 10^{-2}$ M, 2×10^{-3} M). Spectra were allowed to stabilize before adding subsequent drops of $SnCl_2$.

TEM images were obtained at 120 kV on a JEOL JEM-2010 electron microscope at a magnification of 150 000×. TEM samples were prepared by depositing a chlorobenzene solution of TPA-DPA G4 and $(SnCl_2)_{45}$@TPA-DPA G4 (1 μM) on carbon-coated copper grids followed by exposure to RuO_4 vapor for 30 min. HPPS analysis was performed using a Malvern/Sysmex HPP5001 instrument by dynamic light scattering. HPPS samples were prepared by filtering chloroform−acetonitrile (v/v = 1/1) solutions of TPA-DPA G4 and $(SnCl_2)_{45}$@TPA-DPA G4 (1 mg/1 mL) through a membrane filter (0.2 μm) into a clean quartz cell (optical path length, 1 cm; sample height, ∼1 cm). The photocurrent, photovoltage, and $I-V$ curves were measured using an $I-V$ curve tracer (MP-160, Eiko Seiki) under irradiation using a simulated solar light (ESS200, Eiko Seiki; AM 1.5G, 100 mW/cm^2).

Synthesis of 4,4′,4″-Tris(aminophenylthienylphenyl)amine (TPA-NH$_2$, 3). To a solution of tris[4-(2-thienyl)phenyl]amine (**1**, 0.25 g, 0.5 mmol) in anhydrous THF (12.3 mL) cooled at −78 °C was slowly added 1.57 N *n*-butyllithium in hexane (1.3 mL, 2.0 mmol) under a nitrogen atmosphere. The reaction mixture was allowed to warm to room temperature and then stirred for 15 min. The mixture was added to a solution of $ZnCl_2$ (0.30 g, 2.2 mmol) in anhydrous THF (20 mL). 4-Bromonitrobenzene (0.30 g, 1.5 mmol) and $Pd(PPh_3)$ (0.0578 g, 0.05 mmol) were then added to this mixture followed by stirring at room temperature for 24 h. The reaction was quenched by adding the mixture to water (200 mL). Suction filtration gave the crude product **2**, which was washed well with methanol and dried under a vacuum. The residue was treated with $NaBH_2S_3$ (0.39 g, 3 mmol) in anhydrous THF (50 mL) under reflux for 24 h. After the addition of water (50 mL), the pH of the mixture was lowered to 2.5 by the addition of HCl and then neutralized with KOH_{aq} for extraction with dichloromethane (100 mL). The extract was washed with brine and dried using $MgSO_4$. The solvent was evaporated, and the residue was purified by column chromatography on silica gel using a mixture of dichloromethane and ethyl acetate (10:1, v/v) to give the final product **3** as a yellow powder (0.15 g, 41%); ^{1}H NMR (270 MHz, $CDCl_3$, 24 °C, TMS) $\delta = 7.51$ (d, $J = 8.9$ Hz, 6H), 7.43 (d, $J = 8.6$ Hz, 6H), 7.18 (d, $J = 3.8$ Hz, 3H), 7.14 (d, $J = 8.1$ Hz, 6H), 7.11 (d, $J = 3.5$ Hz, 3H), 6.70 (d, $J = 8.6$ Hz, 6H), 3.64 (s, 6H); MS (MALDI-TOF) *m*/*z* 765.8 (M$^+$), calcd 765.02.

Synthesis of TPA-DPA G1. To a mixture of TPA-NH$_2$ (**3**, 72 mg, 93 μmol), benzophenone (136 mg, 0.75 mmol), DABCO (134 mg, 1.2 mmol), and chlorobenzene (10 mL) warmed at 80 °C was added titanium(IV) chloride (60 μL, 0.5 mmol) under a nitrogen atmosphere. The reaction mixture was warmed to 125 °C and stirred overnight. The precipitate was then filtered off, the filtrate was evaporated, and the residue was purified by column chromatography on silica gel using a mixture of hexane, dichloromethane, and ethyl acetate (6:1:1, v/v). Preparative SEC then gave TPA-DPA G1 as a yellow powder (110 mg, 94%); ^{1}H NMR (400 MHz, $CDCl_3$, 25 °C, TMS) $\delta = 7.75$ (d, $J = 7.6$ Hz, 6H), 7.50−7.39 (m, 21H), 7.29−7.25 (m, 9H), 7.15−7.11 (m, 18H), 6.74 (d, $J = 8.4$ Hz, 6H); ^{13}C NMR (100 MHz, $CDCl_3$, 25 °C TMS) $\delta = 168.18$, 150.42, 146.19, 142.89, 142.30, 139.48, 136.05, 130.68, 129.41, 129.29, 129.25, 129.16, 128.63, 128.10, 127.95, 126.33, 125.54, 124.28, 123.21, 123.10, 121.59; IR (KBr, cm^{-1}) 1617 (C═N), 1596 (phenyl), 836, 797, 693; MS (MALDI-TOF) *m*/*z* 1256.7 (M$^+$),

calcd 1257.63. Anal. Calcd for $C_{87}H_{60}N_4S_3$: C, 83.09; H, 4.81; N, 4.45; S, 7.65. Found: C, 82.53; H, 5.18; N, 4.28; S, 7.72.

Synthesis of TPA-DPA G2. To a mixture of TPA-NH_2 (**3**, 76 mg, 100 μmol), DPA dendron G2 (216 mg, 400 μmol), DABCO (134.6 mg, 1.2 mmol), and chlorobenzene (16 mL) warmed at 80 °C was added titanium(IV) chloride (60 μL, 0.5 mmol) under a nitrogen atmosphere. The reaction mixture was warmed to 125 °C and stirred overnight. The precipitate was then filtered off, the filtrate was evaporated, and the residue was purified by column chromatography on silica gel using a mixture of hexane, dichloromethane, and ethyl acetate (6:6:1, v/v). Preparative SEC then gave TPA-DPA G2 as a yellow powder (173 mg, 74%); ^{1}H NMR (400 MHz, $CDCl_3$, 24 °C, TMS) δ = 7.75 (d, J = 8.4 Hz, 6H), 7.71 (d, J = 6.8 Hz, 6H), 7.54−7.50 (m, 12H), 7.47−7.35 (m, 24H), 7.27 (m, 6H), 7.23−7.14 (m, 30H), 7.01 (m, 6H), 6.87 (d, J = 8.4 Hz, 6H), 6.73 (d, J = 8.4 Hz, 6H), 6.63 (d, J = 8.8 Hz), 6.58 (d, J = 8.4 Hz, 6H); ^{13}C NMR (100 MHz, $CDCl_3$, 25 °C, TMS) δ = 168.72, 168.25, 167.88, 153.52, 151.61, 150.82, 146.16, 143.12, 142.088, 139.19, 139.00, 135.75, 135.56, 134.36, 130.83, 130.77, 129.93, 129.90, 129.54, 129.28, 129.24, 129.20, 128.77, 128.70, 128.52, 128.06, 127.92, 127.70, 126.30, 125.42, 124.30, 123.24, 122.90, 121.76, 120.44, 120.22; IR (KBr, cm^{-1}): 1615 (C═N), 1590 (phenyl), 843, 798, 697; MS (MALDI-TOF) m/z 2332.4 (M^+), calcd 2332.94; Anal. Calcd for $C_{165}H_{114}N_{10}S_3$: C, 84.95; H, 4.93; N, 6.00; S, 4.12. Found: C, 84.39; H, 5.04; N, 5.75; S, 4.29.

Synthesis of TPA-DPA G3. To a mixture of TPA-NH_2 (**3**, 76 mg, 100 μmol), DPA dendron G3 (503 mg, 400 μmol), DABCO (134.6 mg, 1.2 mmol), and chlorobenzene (16 mL) warmed at 80 °C was added titanium(IV) chloride (60 μL, 0.5 mmol) under a nitrogen atmosphere. The reaction mixture was warmed to 125 °C and stirred overnight. The precipitate was then filtered off, the filtrate was evaporated, and the residue was purified by column chromatography on silica gel using a mixture of hexane, dichloromethane, and ethyl acetate (5:5:1, v/v). Preparative SEC then gave TPA-DPA G3 as a yellow powder (309 mg, 69%); ^{1}H NMR (400 MHz, $CDCl_3$, 24 °C, TMS) δ = 7.74−7.71 (m, 24H), 7.55−6.52 (m, 198H); ^{13}C NMR (100 MHz, $CDCl_3$, 25 °C, TMS) δ = 168.74, 168.55, 168.25, 168.21, 168.012, 167.95, 167.73, 153.95, 153.62, 153.53, 151.95, 151.75, 139.10, 138.96, 138.83, 135.67, 135.60, 135.49, 134.23, 134.10, 133.86, 130.78, 130.52, 130.21, 130.04, 129.95, 129.25, 128.89, 128.67, 128.50, 128.05, 127.89, 127.70, 127.60, 127.34, 126.22, 125.47, 125.37, 124.19, 123.20, 123.07, 121.99, 121.72, 120.74, 120.39, 120.19, 119.84; IR (KBr, cm^{-1}) 1617 (C═N), 1582 (phenyl), 836, 797, 693; MS (MALDI-TOF) m/z 4483.1 (M^+), calcd 4483.54. Anal. Calcd for $C_{321}H_{222}N_{22}S_3$: C, 85.99; H, 4.99; N, 6.87; S, 2.15. Found: C, 85.53; H, 5.14; N, 6.63; S, 2.16.

Synthesis of TPA-DPA G4. To a mixture of TPA-NH_2 (**3**, 76 mg, 100 μmol), DPA dendron G4 (1.07 g, 400 μmol), DABCO (134.6 mg, 1.2 mmol), and chlorobenzene (16 mL) warmed at 80 °C was added titanium(IV) chloride (60 μL, 0.5 mmol) under a nitrogen atmosphere. The reaction mixture was warmed to 125 °C and stirred overnight. The precipitate was then filtered off, the filtrate was evaporated, and the residue was purified by preparative SEC to give TPA-DPA G4 as a yellow powder (591 mg, 67%); ^{1}H NMR (400 MHz, $CDCl_3$, 25 °C, TMS) δ = 7.75−6.73 (m, 438H); ^{13}C NMR (100 MHz, $CDCl_3$, 25 °C, TMS) δ = 168.79, 168.60, 168.31, 168.17, 168.03, 167.84, 155.01, 153.62, 152.03, 151.75, 139.14, 138.92, 138.63, 135.69, 135.51, 135.32, 134.32, 134.06, 133.84, 130.77, 130.47, 130.24, 129.96, 129.62, 129.36, 129.25, 128.69, 128.43, 128.06, 127.90, 127.72, 126.18, 125.45, 124.16, 123.42, 123.05, 122.18, 121.98, 120.95, 120.74, 120.39, 120.16, 119.92, 119.85; IR (KBr, cm^{-1}) 1614 (C═N), 1577 (phenyl), 847, 785, 695; MS (MALDI-TOF) m/z 8782.7 (M^+), calcd 8784.76. Anal. Calcd for $C_{633}H_{438}N_{46}S_3$: C, 86.55; H, 5.03; N, 7.33; S, 1.10. Found: C, 86.06; H, 5.48; N, 7.08; S, 1.19.

Synthesis of TPA-DPA G5. To a mixture of TPA-NH_2 (**3**, 38 mg, 50 μmol), DPA dendron G5 (1.11 g, 200 μmol), DABCO (134.6 mg, 1.2 mmol), and chlorobenzene (100 mL) warmed at 80 °C was added titanium(IV) chloride (60 μL, 0.5 mmol) under a nitrogen atmosphere. The reaction mixture was warmed to 125 °C and stirred overnight. The precipitate was then filtered off, the filtrate was evaporated, and the residue was purified by preparative SEC to give TPA-DPA G5 as a yellow powder (98 mg, 11%); ^{1}H NMR (400 MHz, $CDCl_3$, 25 °C, TMS) δ = 7.75−6.73 (m, 870H); ^{13}C NMR (100 MHz, $CDCl_3$, 25 °C, TMS) δ = 168.81, 168.55, 168.27, 168.00, 167.83, 167.69, 154.03, 153.61, 152.53, 151.77, 139.17, 138.95, 138.64, 135.66, 135.46, 134.12, 130.80, 130.47, 129.99, 129.27, 128.72, 128.08, 127.92, 127.78, 120.76, 120.41, 120.19, 119.91; IR (KBr, cm^{-1}) 1614 (C═N), 1577 (phenyl), 847, 785, 695; MS (MALDI-TOF) m/z 17393.3 (M^+), calcd 17387.18. Anal. Calcd for $C_{1257}H_{870}N_{94}S_3$: C, 86.83; H, 5.04; N, 7.57. Found: C, 86.06; H, 5.48; N, 7.08.

Preparation of the Photoelectrode. TiO_2 paste (Ti−Nanoxide D) was deposited onto a glass sheet coated with a fluorine-doped stannic oxide layer (sheet resistance, 10 Ω/cm^2) using a "squeegee" technique. The heated electrodes were impregnated with a 0.05 M titanium(IV) chloride solution in a water-saturated desiccator for 30 min at 70 °C, washed with distilled water, and heated for 10 min at 450 °C in air. The hot electrodes were allowed to cool to 100 °C and then immediately soaked in a mixture solution of acetonitrile/1-propanol (1:1, v/v) containing *cis*-bis(isothiocyanato)bis(2,2′ bipyridyl-4,4′-dicarboxylato)-ruthenium(II) bis-tetrabutylammonium (N719) dye. The concentration of this solution was maintained at a minimum of 3×10^{-4} M.[2a]

Fabrication of the DSSC. The DSSC was fabricated in air as a sandwich-type open electrochemical cell composed of a dye-adsorbed TiO_2 electrode, a spacer, and a Pt counter electrode. The electrolyte solution for analysis was composed of 0.6 M dimethylpropylimidazolium iodide (DMP II), 0.05 M iodine, and 0.1 M lithium iodide in 3-methoxypropionitrile (MPN). The dye-coated semiconductor film was illuminated through a conducting glass support with a mask.

Acknowledgment. The authors extend their gratitude to Dr. H. Arakawa and Dr. T. Yamaguchi for useful suggestions on DSSC fabrication and to Mr. M. Minoda for support in DSSC measurements. And we also thank Dr. J-S. Cho and Dr. M. Higuchi for their suggestions on our work. This work was supported in part by the Core Research for Evolutional Science and Technology (CREST) program of the Japan Science and Technology (JST) Agency, by a Grant-in-Aid for Scientific Research (No. 15350073) offered under the 21st Century Center of Excellence (COE) program (Keio-LCC) of the Ministry of Education, Culture, Sports, Science and Technology (MEXT) of Japan, and by a research grant (Project No. 23) from the Kanagawa Academy of Science and Technology (KAST).

Supporting Information Available: Additional data provided in PDF file. This material is available free of charge via the Internet at http://pubs.acs.org.

JA050765C